

# Microstructure, Friction and Wear Behavior and Corrosion Resistance of electroless Double-Layer Ni-P/Ni-Mo-P Coatings on AZ91D Magnesium Alloy

Jingpei Liu<sup>a</sup> , Wanchang Sun<sup>a\*</sup> , Eryong Liu<sup>a</sup>, Xiaojia Liu<sup>a</sup> , Congxiao Zhang<sup>a</sup>, Yifan Xu<sup>a</sup>,  
Mengran Zhou<sup>a</sup>, Bo Zhang<sup>a</sup>, Hui Cai<sup>a</sup>, Jingli Zhang<sup>a</sup>

<sup>a</sup>Xi'an University of Science and Technology, College of Materials Science and Engineering, 710054, Xi'an, Shaanxi, China.

Received: August 25, 2023; Revised: November 16, 2023; Accepted: December 12, 2023

Double-layer Ni-P coatings with low phosphorus content in the inner layer and high phosphorus content in the outer layer and Ni-Mo-P composite coatings are successfully prepared on the surface of AZ91D magnesium alloy by chemical plating process. The microstructures, friction and corrosion resistance of double-layer Ni-P and Ni-Mo-P coatings are studied in comparison. Meanwhile, the deposition and corrosion resistance mechanism for the coatings are investigated. Results convey that both Ni-P and Ni-Mo-P coatings showcase an amorphous structure. The coating possesses denser and more homogeneous structure with the co-doping of Mo. The micro-indentation hardness (859.7 HV) and friction coefficient (0.58) of Ni-Mo-P coatings show that the ternary alloy coating is firmly bonded to the magnesium alloy substrate. Besides, the Ni-Mo-P coatings demonstrate exceptional wear resistance attributed to Mo co-deposition, fostering grain refinement and facilitating the growth of passivation films.

**Keyword:** Ni-P/Ni-Mo-P coating, electroless plating, microstructure, friction and wear behavior, corrosion resistance.

## 1. Introduction

Magnesium and its alloys, known as the “green engineering materials” in the new century, are undergoing thorough sufficiently investigation in diverse industries like mechanical industry, medical devices, electronic equipment and aerospace by virtue of their unique advantages incorporating low density, high specific strength, fast electrical conductivity and excellent electromagnetic shielding properties<sup>1-3</sup>. Unfortunately, the high chemical activity of magnesium poses challenges, with oxidation and corrosion emerging as primary concerns in applications, significantly impeding the advancement of magnesium alloys in high-precision industries<sup>4-6</sup>. To address these challenges, surface processing approach including surface modification, chemical conversion coatings and electrophoretic deposition have been recognized as attractive strategies to enhance the wear and corrosion resistance of magnesium alloys. Among these methods, chemically or electrochemically converted films are preferred to form a stable compound coating because of the low-cost and practical, which improves the performance and service life of the material<sup>2,7,8</sup>.

In the contemporary landscape of highly developed industries, the advancement of surface treatment processes, particularly the chemical Ni-P coating, has gained significant prominence for various alloy surfaces<sup>9,10</sup>. Electroless Ni-P alloy coating is characterized with uniform thickness and superior mechanical and chemical properties, thanks to the seamless integration between the coating and the matrix.

Especially in multilayer coatings, the double-layer Ni-P coating with different phosphorus content in the inner and outer layers meets the exacting demands across various industrial applications<sup>11-13</sup>. However, binary alloy coatings fall short in addressing the challenges in the present harsh environment, so the integration of third elements into Ni-P alloys becomes imperative, with the aim of obtaining high performance ternary alloy coatings<sup>14,15</sup>. The surface morphology and properties of Ni-P and Ni-Mo-P composite coatings are comparatively studied by Liu and Liu<sup>16</sup>, which revealed that the surfaces of both coatings are composed of “cytosol” structure characterized by irregular sizes. Wu et al.<sup>17</sup> successfully deposited Ni-Mo-P coatings on SiO<sub>2</sub> substrates and found that the coating effectively blocked the corrosion relationship between the coating and the environment.

Therefore, the center of this study is to comparatively evaluate the properties of the double-layer Ni-P coating and the Ni-Mo-P composite coating. Additionally, we aim to discuss the deposition process and elucidate the corrosion resistance mechanisms inherent in these coatings.

## 2. Materials and Methods

### 2.1. Pretreatments

AZ91D magnesium alloys with the specifications of 18 mm×16 mm×12 mm, adopted as the substrates, were polished with water sandpaper of 180, 600, 800, 1000, 1500, 2000 grit sequentially to eliminate oxidation layer and impurities.

\*e-mail: [sunwanchang@tsinghua.org.cn](mailto:sunwanchang@tsinghua.org.cn)

Then, the substrates were dipped into acetone solution and alkaline solution (50 g/L sodium hydroxide and 20 g/L sodium phosphate, 50°C, 10min) in turn to remove oil thoroughly. Acidic solution formulated with 40 g/L phosphoric acid and 5 g/L potassium fluoride was used to eradicate the oxides left after sandpaper sanding. After acid washing, the specimens were placed in activation solution (170 ml/L hydrofluoric acid and 30 g/L sodium fluoride) to produce a protective film. For subsequent chemical plating, stannate conversion treatment must be applied to the magnesium alloy surface to form a pre-plating layer. Finally, the matrix can be chemically plated after three steps of sensitization, activation and reduction.

### 2.2. Preparation of double-layer Ni-P and Ni-Mo-P coatings

The treated samples were placed in a configured electroless bath to deposit double-layer Ni-P coatings and Ni-Mo-P coatings. Details of electroless plated double-layer Ni-P/Ni-Mo-P coatings are arranged in Table 1. The experimental flow is shown in Figure 1.

### 2.3. Characterization

The surface and cross-section morphologies of the coatings were observed by scanning electron microscopy (JSM-6390A, Japan), equipped with energy dispersive spectroscopy (EDS) was used to describe the chemical composition. The phase structure of the plated layers was analyzed by X-ray photoelectron spectroscopy (XRD, XRD-7000). The tribological behavior was performed with the reciprocating friction and wear tester (MMW-10) under a load of 20 N and time of 10 min. The corrosion resistance of the coatings was investigated using an electrochemical workstation and the data were fitted by Z-View software.

## 3. Results and Discussion

### 3.1. Deposition mechanism for Ni-Mo-P composite coatings

To investigate the mechanism of electroless plating, the adsorption and growth process of Ni-Mo-P composite coatings displayed in Figure 2 is discussed in the following stages. First of all, a majority of the dispersed particles suspended in the liquid phase migrate to the plated surface via solution flow (e.g., stirring) to undergo reversible physical adsorption, while another fraction moves directly from suspension to a strongly adsorbed state. Subsequently, in the stage of physical adsorption into chemisorption,  $\text{Ni}^{2+}$  and  $\text{H}_2\text{PO}_2^-$  selectively adsorb anions and cations in the solution, which are then reduced to metallic nickel and phosphorus deposited on the matrix surface by redox reactions with strong reducing agents. As the complexing agent equilibriums in the electrode potential of nickel and molybdenum,  $\text{MoO}_4^{2-}$  induces co-deposition with  $\text{Ni}^{2+}$  ions on the foundation of the co-deposition of nickel and phosphorus<sup>18</sup>. Finally, with the continuous reaction, the Ni-Mo-P layer grows until it covers the entire substrate during the reduction and deposition of metal ions onto the surface. The detailed reaction equation is as follows:

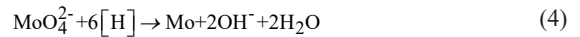
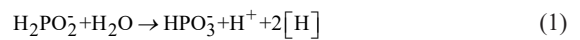


**Table 1.** Compositions and parameters for electroless plating.

Coating	Solution composition	PH	Temperature [°C]	Time [min]
Pre-plating	20 g/L stannate			
	10 g/L sodium hydroxide			
	40 g/L sodium pyrophosphate			
	5 g/L sodium acetate			
Ni-P coating (Low phosphorus layer)	15 g/L nickel sulfate	5.3	72	60
	10 g/L sodium hypophosphite			
	18 g/L citric acid			
	5 g/L lactic acid			
Ni-P coating (High phosphorus layer)	10 g/L ammonium hydro fluoride	5.3	72	60
	15 g/L nickel sulfate			
	20 g/L sodium hypophosphite			
	18 g/L citric acid			
Ni-Mo-P coating	5 g/L lactic acid	7.5	65	60
	10 g/L ammonium hydro fluoride			
	10 g/L nickel sulfate			
	0.2, 0.3, 0.4, 0.5, 0.6 g/L sodium molybdate			
	35 g/L sodium hypophosphite			
	20 g/L sodium citrate			
	10 g/L sodium acetate			

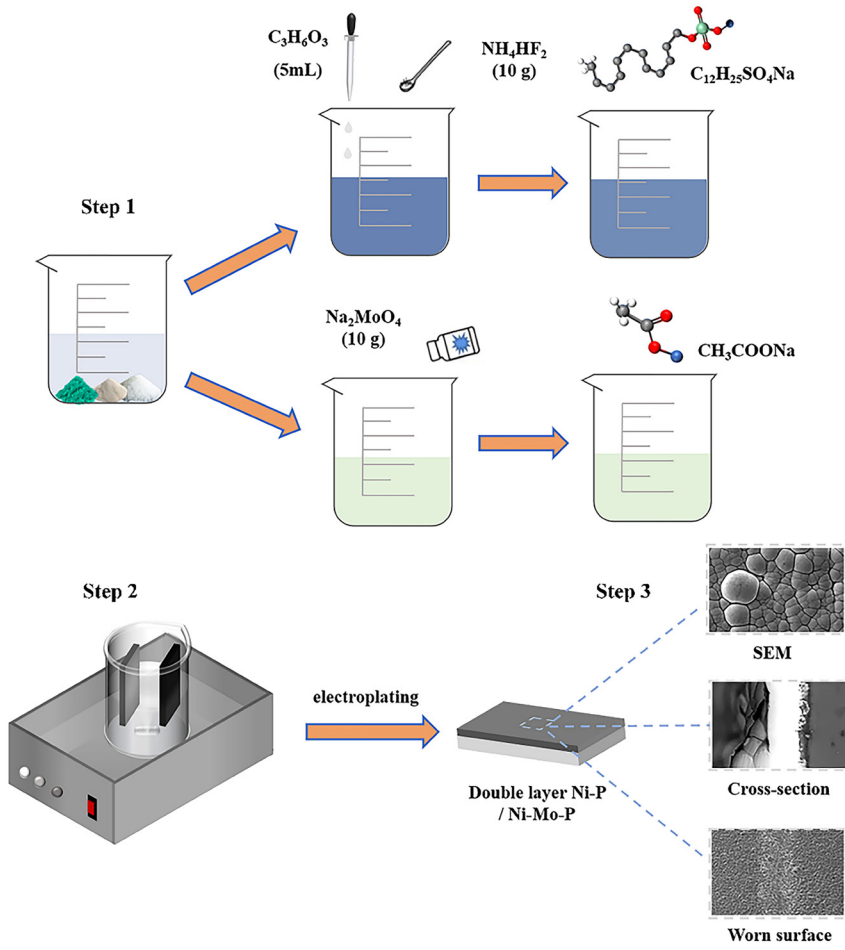


Figure 1. Schematic diagram of the experimental process.

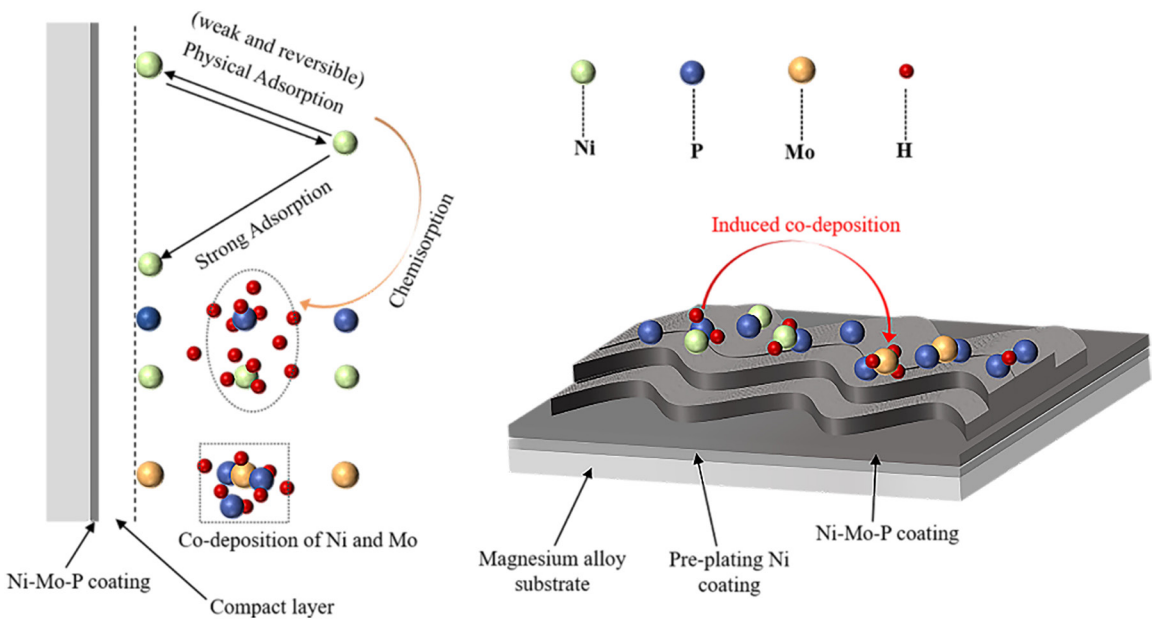


Figure 2. Schematic diagram of adsorption and growth mechanisms for Ni-Mo-P coatings.

### 3.2. Morphological characteristics of double-layer Ni-P and Ni-Mo-P coatings

The surface morphologies of double-layer Ni-P and Ni-Mo-P coatings are presented in Figure 3, exhibiting a homogeneous morphology with typical cell-like structure. Comparatively, the cellular organization of Ni-Mo-P coating is finer, denser, and more uniformly arranged than that of

double-layer Ni-P coating. This may be related with the co-deposited of element Mo that as a hard and tough metallic element reduces the size of cellular tissue. Meanwhile, the coatings completely cover the surface of the magnesium alloy substrate without defects such as cracks and peeling.

The cross-sectional morphologies and line EDS analyses of double-layer Ni-P and Ni-Mo-P coatings given in Figure 4

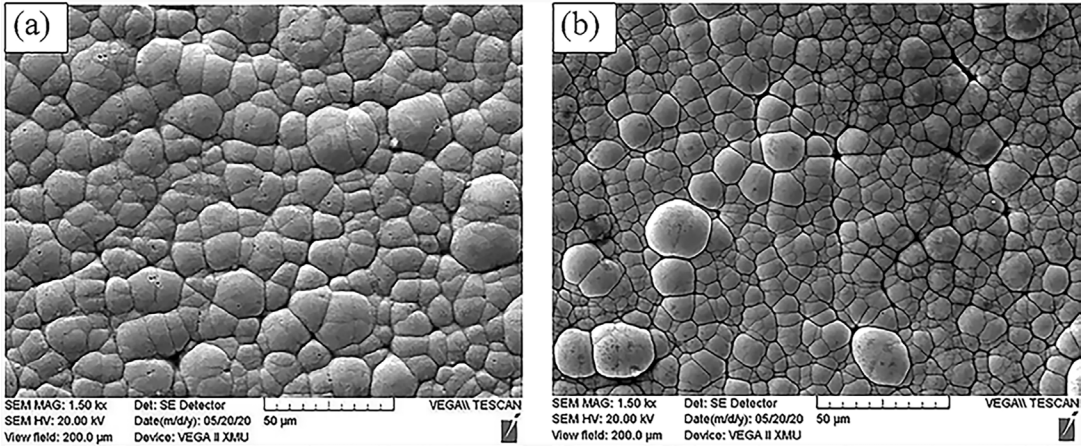


Figure 3. Surface morphologies of double-layer Ni-P and Ni-Mo-P coatings double-layer Ni-P coating (b) Ni-Mo-P coating.

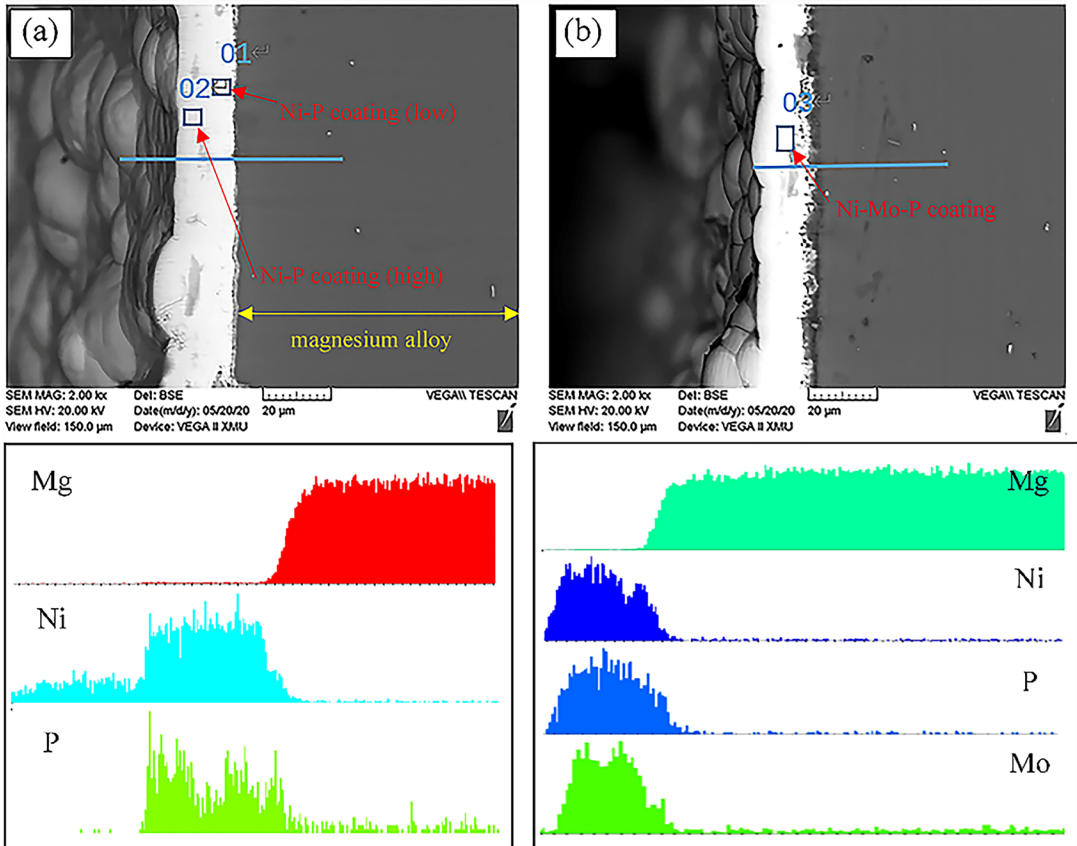


Figure 4. The cross-sectional morphologies and line EDS of the coatings double-layer Ni-P coating (b) Ni-Mo-P coating.

reflect that Ni, Mo and P elements have been successfully doped into the matrix. From Figure 4a without mixing with Mo elements, we can observe that the gray-black cell-like structure on the left is the coating area and the gray section on the right is the magnesium alloy matrix, where the content of phosphorus at positions 1 and 2 is listed in Table 2. It is found that the inner layer exhibits a lower phosphorus content (4.46 wt%) than the outer layer (13.13 wt%), underscoring the successful preparation of a double-layer Ni-P coating featuring low phosphorus in the inner layer and high phosphorus in the outer layer on the substrate surface. By comparing Figure 4b with Figure 4a, Ni, P and Mo components are detected in the plated layer, where phosphorus and molybdenum particles are uniformly dispersed in the Ni matrix that leads to a homogeneous impurity-free bonding interface between the coating and the matrix. Moreover, the amount of phosphorus in the Ni-Mo-P coating (position 3) is 10.62 wt% ranging from Ni-P bilayer phosphorus content. Nevertheless, the dosage of Mo element does not remarkably change the structure of the coatings.

Figure 5 compares the X-ray diffraction spectra of double-layer Ni-P coating and Ni-Mo-P coating. Obviously, there is a wider broad peak of Ni appeared at  $2\theta \approx 45^\circ$  with (111) miller indices, which indicates that the coatings are amorphous structures. In contrast, the diffraction peak and peak area of the double-layer Ni-P coating are smaller than those of the Ni-Mo-P ternary alloy plating because the atomic radius of Mo is larger than that of Ni during the solid solution formation by molybdenum and nickel co-deposition, resulting in a larger crystal plane spacing. The results reveal that molybdenum doping is beneficial to improve the degree of amorphous state of the plating, thereby enhancing the corrosion resistance.

### 3.3. Micro-indentation hardness of double-layer Ni-P and Ni-Mo-P coatings

It can be observed from the micro-indentation hardness graph of double-layer Ni-P and Ni-Mo-P coatings shown in Figure 6, the microhardness of Ni-Mo-P coating peaks at an impressive 859.7 HV and the hardness of double-layer Ni-P coating is only 546.325 HV. This discrepancy serves as compelling evidence that the Ni-Mo-P coating effectively safeguards the magnesium alloy substrate. The increase in microhardness of Ni-Mo-P plating is attributed to the Hall-Petch effect [30], indicating an inverse relationship between grain size and microhardness, and the incorporation of molybdenum element precipitates fine Ni/Ni-Mo reinforced phase within the coating. It is the deposition of the second reinforced phase that reduces the grain size of the composite coating and increases the number of grain boundaries, which is consistent with the results exhibited in Figure 3b.

### 3.4. The friction and wear behaviors of double-layer Ni-P and Ni-Mo-P coatings

Figure 7 describes the variation of the friction coefficient for the coatings over sliding time. The results show that the friction coefficient curves initially increase and then tend to stabilize with values fluctuating in the range of 0.5 to 0.7, owing to the fact that the rough surface at the beginning of the test increases the friction coefficient and the worn surface becomes smooth as the test progresses. After comparison, the average friction coefficient of double-layer Ni-P coating is about 0.67 during the stable wear period, while the average friction coefficient of the coating doped with Mo elements is about 0.58, lower than that of the Ni-P coating. Furthermore, the Ni-Mo-P coating displays a short-term break-in period, as shown by a decreasing trend of the friction coefficient at 1 minute.

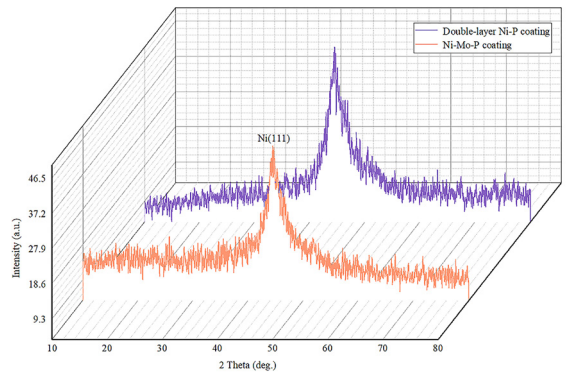


Figure 5. XRD patterns of double-layer Ni-P and Ni-Mo-P coatings.

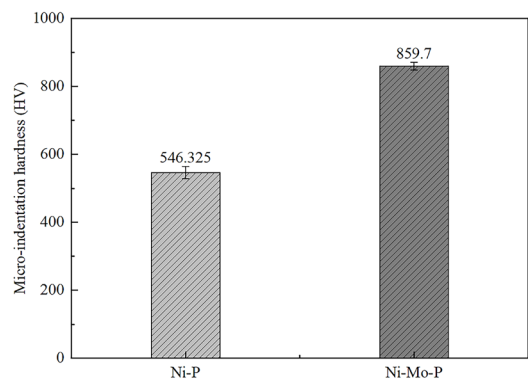


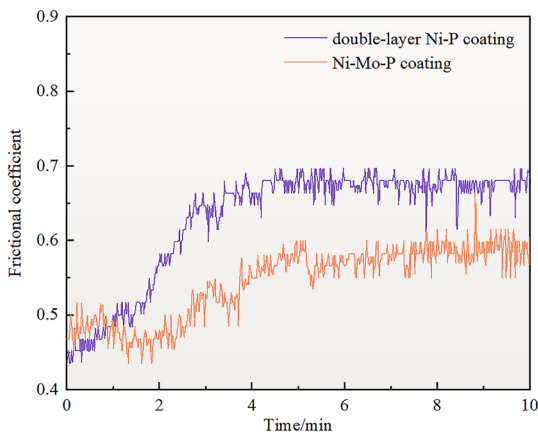
Figure 6. Micro-indentation hardness of double-layer Ni-P and Ni-Mo-P coatings.

Table 2. Energy spectrum analysis of the coatings.

Sample	Number	Content of Ni (wt%)	Content of P (wt%)	Content of Mo (wt%)
Ni-P coating	01	95.54	4.46	
	02	86.87	13.13	
Ni-Mo-P coating	03	84.20	10.62	5.18

Although the microstructure has not yet been changed completely, the hard molybdenum particles can play a load-bearing role in the frictional wear process. When the coating is worn out, the shed Mo and its deposits adhere to the friction surface and resist the impact and wear on the plated surface caused by the frictional subsets, so that to optimize the friction reduction and anti-wear performance.

The worn morphologies of the coatings are shown in Figure 8. At the same magnification, A wider wear track can be observed in Figure 8a, accompanied by noticeable microcracks and bumpy undulations on the wear surface. Hence, the Ni-P coating exhibits a severe wear condition with lots of abrasive grains and chips on the surface of the abrasion marks, which implies that the coating is



**Figure 7.** Friction coefficient of double-layer Ni-P and Ni-Mo-P coatings in room temperature and atmospheric pressure.

plastically deformed to a large extent during the frictional wear process. By contrast, the SEM image of abrasion marks after the introduction of Mo particles is displayed in Figure 8b, where it can be seen that the width of the abrasion marks becomes narrower and the color gets lighter, with almost no presence of a peeling layer or abrasive chips. The wear mechanism is primarily abrasive wear accompanied by slight adhesive wear. This result is accounted for by the smooth and dense morphology of the Ni-Mo-P coating. In addition, the Ni-Mo solid solution formed through the co-deposition of molybdenum and nickel possesses a friction-reducing effect improved the wear resistance of the coating.

### 3.5. Corrosion resistance of double-layer Ni-P and Ni-Mo-P coatings

Figure 9 shows the polarization curves of double-layer Ni-P and Ni-Mo-P coating. An evident positive shift in the corrosion potential of the Ni-Mo-P coating, compared to the double-layer Ni-P coating, suggests a lower tendency to corrosion in the Ni-Mo-P plating. The self-corrosion potential and self-corrosion current density of the corresponding coatings obtained by the Tafel curve extrapolation method are described in Table 3, we can observe that the corrosion potential of Ni-Mo-P coating as  $-0.9269$  V, with a corrosion current of  $2.3154 \times 10^{-5}$  A/cm<sup>2</sup>. According to  $E_{\text{corr}}$  reflects the trend of metal corrosion and  $I_{\text{corr}}$  represents the kinetics of metal corrosion process can be further derived from Ni-Mo-P coating with superior corrosion resistance<sup>19</sup>. The reasons for this phenomenon are mainly divided into the following aspects. First, classical corrosion theory<sup>20</sup> suggests that the second phase generally reduces the corrosion resistance of the material because multiphase alloys with various potential differences are susceptible to form corrosion microcells in corrosive media.

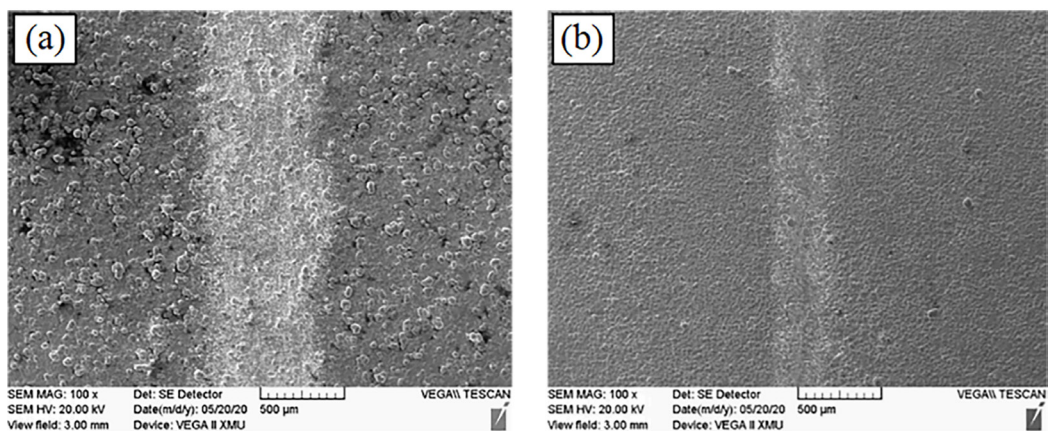
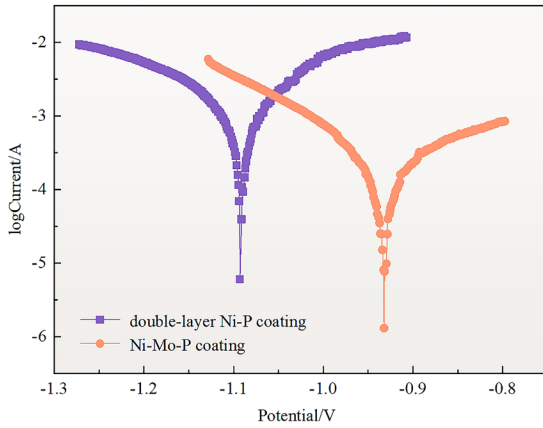


**Figure 8.** Friction and scratch morphologies of the coatings double-layer Ni-P coating (a) Ni-P coating (b) Ni-Mo-P coating.

**Table 3.** The corrosion parameters for test of the coatings.

Sample	$E_{\text{corr}}$ (V <sub>SCE</sub> )	$I_{\text{corr}}$ (A/cm <sup>2</sup> )
Ni-P coating	-1.0919	$8.1356 \times 10^{-4}$
Ni-Mo-P coating	-0.9269	$2.3154 \times 10^{-5}$

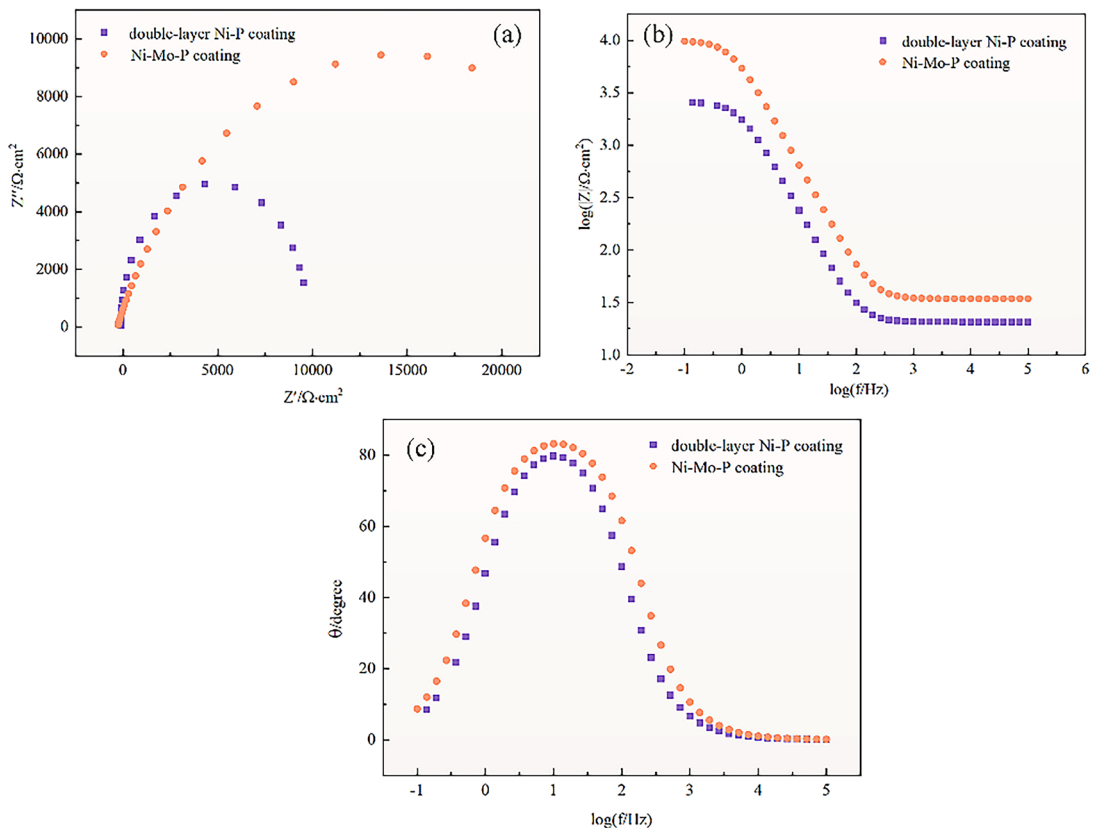
However, the present experimental results demonstrate that the Ni-Mo-P plating with mixed crystal structure is conducive to rapid formation of a uniform anodic passivation film in the corrosive environment of alloy plating. Moreover, the addition of Mo refines the microstructure and decreases the porosity of the coating, increasing the densities of Ni-Mo-P coating and diminishing the probability of forming corrosion microporous.



**Figure 9.** Polarization curves of double-layer Ni-P and Ni-Mo-P coatings.

In order to further evaluate the difference in corrosion degree between the coatings, the Nyquist diagram and Bode diagrams are presented in Figure 10. Figure 10a shows that the capacitive arc resistance radius of the Ni-Mo-P coating differs from that of the double-layer Ni-P coating, indicating that Ni-Mo-P coatings are more resistant to corrosion. Additionally, the presence of a capacitive arc in the Nyquist plot supposes that the time constant of electrochemical impedance spectrum is 1. The impedance spectrum fitting results in Table 4 reveal that  $R_{ct}$  values of the Ni-P coating and the Ni-Mo-P coating are  $1.06 \times 10^4 \Omega \cdot \text{cm}^2$  and  $1.91 \times 10^4 \Omega \cdot \text{cm}^2$ , respectively. In Figure 10b, the general shape of the graph remains unchanged, which reveals that the coating has not suffered severe corrosion damage. The Ni-Mo-P coating possesses stronger corrosion resistance since the  $|Z|$  value of the Ni-Mo-P coating is bigger than that of the Ni-P coating. A smooth bun peak appeared in Figure 10c implies that the coatings effectively impede contact between the magnesium alloy substrate and the corrosive media.

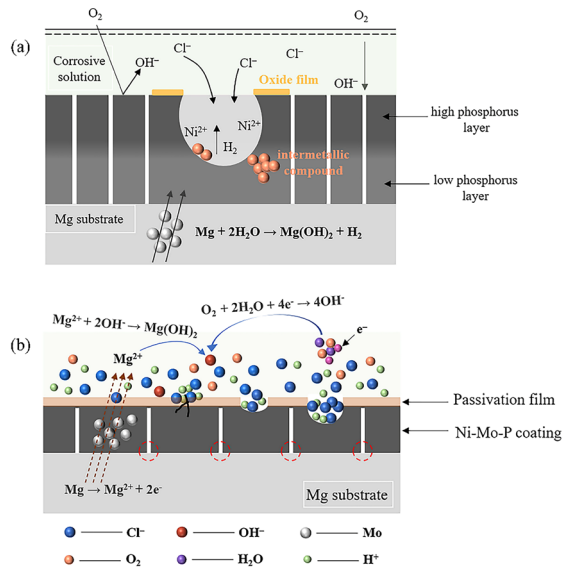
The corrosion modes of double-layer Ni-P and Ni-Mo-P coatings in acidic solutions include uniform corrosion and pitting corrosion, as shown in Figure 11<sup>21,22</sup>. Uniform corrosion arises from the reaction between  $\text{H}^+$  and  $\text{Ni}^{2+}$  in acidic solutions. According to the principle of corrosion electrochemistry, the active  $\text{Cl}^-$  preferentially adsorbed at weak sites on the coating surface (around pores and cell boundaries) disrupts the dynamic equilibrium of Ni conversion to  $\text{Ni}^{2+}$  and produces soluble  $\text{NiCl}_2$ .



**Figure 10.** The Nyquist diagrams (a) and Bode diagrams (b-c) of the coatings.

**Table 4.** Electrochemical parameters from EIS data of the coatings.

Sample	$R_s$ ( $\Omega \cdot \text{cm}^2$ )	$Y_{0,dl}$ ( $\text{S}^{\alpha} \cdot \Omega^{-1} \cdot \text{cm}^{-2}$ )	n	$R_{ct}$ ( $\Omega \cdot \text{cm}^2$ )
Ni-P coating	13.52	$1.35 \times 10^{-4}$	0.88	$1.06 \times 10^4$
Ni-Mo-P coating	12.86	$2.06 \times 10^{-4}$	0.83	$1.91 \times 10^4$

**Figure 11.** Schematic diagram of corrosion resistance mechanisms for the coatings double-layer Ni-P coating (b) Ni-Mo-P coating.

When the pitting potential is reached, a pitting nucleus forms in the weak region, marking the beginning of corrosion. The reason why the coating has excellent corrosion resistance is because the amorphous chemical coating has a uniform structure, fewer defects, and a uniform electrode potential, which facilitates the formation of a uniform and defect free corrosion passivation film during the corrosion process and prevents the occurrence of corrosive micro batteries. In addition, the metalloid element P accelerates the growth of surface passivation films in sodium chloride medium. The outstanding corrosion resistance of the coatings is contributed to the fact that amorphous chemical coatings characterized by homogeneous structure and few defects have uniform electrode potentials, therefore, it is convenient to form uniform and defect-free corrosion passivation films during the corrosion process and prevent the occurrence of corrosion microcells. Subsidiarily, the metalloid element P accelerates the growth of surface passivation films in sodium chloride media. The passivation film discourages the dissolution of reactive substances, diminishes the corrosion rate of metals and improves the protective performance of the chemical coatings. Nevertheless, Ni-Mo-P coatings exhibit better corrosion resistance because the co-deposition of Mo with Ni and P not only preserves the amorphous state structure, but also refines the organization and enhances the resistance to  $\text{Cl}^-$  corrosion.

#### 4. Conclusions

The Ni-Mo-P composite coatings processed by chemical plating method show superior mechanical properties and

corrosion resistance in comparison to the double-layer Ni-P coatings. The detailed results are as follows:

- (1) The Ni-Mo-P coating has a finer, denser and more orderly organization than that of the double-layer Ni-P coating, which are mainly attributed to the effective promotion and refinement of nucleation by Mo.
- (2) The XRD pattern shows that both coatings are amorphous, and the molybdenum doping is beneficial to improve the degree of amorphous state of the alloy coating and enhance the corrosion resistance. Benefiting from the optimized microstructure, higher microhardness (859.7 HV) is obtained for Ni-Mo-P coating.
- (3) For Ni-Mo-P composite coating, the  $E_{\text{corr}}$  is -0.9269 V and the  $I_{\text{corr}}$  is  $2.3154 \times 10^{-5} \text{ A} \cdot \text{cm}^{-2}$ . Therefore, molybdenum co-deposited with nickel and phosphorus allows the Ni-Mo-P coating to exhibit better corrosion resistance than the double-layer Ni-P coating.

#### 5. Acknowledgments

This work was supported by the National Natural Science Foundation of China under Grant number 50172023; the Shaanxi Industrial Science and Technology Research under Grant number 2014K08-09; and the Key Research and Development Program of Shaanxi Province of China under Grant number 2020GY-115.

#### 6. References

1. Shi L, Hu J, Lin XD, Fang L, Wu F, Xie J, et al. A robust superhydrophobic PPS-PTFE/SiO<sub>2</sub> composite coating on AZ31 Mg alloy with excellent wear and corrosion resistance properties. *J Alloys Compd.* 2017;721:157-63.
2. Dong YR, Sun WC, Liu XJ, Jia ZW, Guo F, Ma M, et al. Effect of CNTs concentration on the microstructure and friction behavior of Ni-GO-CNTs composite coatings. *Surf Coat Tech.* 2019;359:141-9.
3. Scharf C, Ditzel A, Shkurankov A, Morales E, Blawert C, Dietzel W, et al. Corrosion of AZ91 secondary magnesium alloy. *Adv Eng Mater.* 2005;7(12):1134-42.
4. Huang HL, Yang WL. Corrosion behavior of AZ91D magnesium alloy in distilled water. *Arab J Chem.* 2020;13(7):6044-55.
5. Coy AE, Viejo F, Skeldon P, Thompson GE. Susceptibility of rare-earth-magnesium alloys to micro-galvanic corrosion. *Corros Sci.* 2010;52(12):3896-906.
6. Mousavi ASH, Masoud S, Roghani ZM. The effect of electroless bath parameters and heat treatment on the properties of Ni-P and Ni-P-Cu composite coatings. *Mater Res.* 2018;21(2):e20170973.
7. Wu W, Zhang F, Li YC, Song L, Chen DC. Corrosion resistance of dodecanethiol-modified magnesium hydroxide coating on AZ31 magnesium alloy. *Appl Phys, A Mater Sci Process.* 2019;126(1):1-11.
8. Karthikeyan S, Vijayaraghavan L. Investigation of the surface properties of heat treated electroless Ni-P coating. *Trans IMF Int J Surf Eng Coat.* 2016;94(5):265-73.

9. Ger MD, Hwang BJ. Effect of surfactants on codeposition of PTFE particles with electroless Ni-P coating. *Mater Chem Phys.* 2002;76(1):38-45.
10. Shu X, He Z, Wang YX, Yin L. Mechanical properties of Ni-based coatings fabricated by electroless plating method. *Surf Eng.* 2020;36(9):944-51.
11. Tian SS, Sun WC, Liu YW, Xiao Y, Jia YP. Microstructures and corrosion resistance of conversion film-electroless Ni-W-P ternary coatings on AZ91D magnesium alloy. *Trans IMF Int J Surf Eng Coat.* 2021;99(6):292-8.
12. Bahadormanesh B, Ghorbani M. Ni-P/Zn-Ni compositionally modulated multilayer coatings – Part 1: electrodeposition and growth mechanism, composition, morphology, roughness and structure. *Appl Surf Sci.* 2018;442:275-87.
13. Ren L, Cheng YH, Yang JY, Wang QG. Study on heat transfer performance and anti-fouling mechanism of ternary Ni-W-P coating. *Appl Sci.* 2020;10(11):3905.
14. Sarika S, Abhilash S, Sumi VS, Rijith S. Synthesis and characterization of transition metal mixed oxide doped graphene embedded durable electrocatalyst for hydrogen evolution reaction. *Int J Hydrogen Energy.* 2021;46(30):16387-403.
15. Song GS, Sun S, Wang ZC, Luo CZ, Pan CX, Physicstechnology SO, et al. Synthesis and characterization of electroless Ni-P/Ni-Mo-P duplex coating with different thickness combinations. *Acta Metall Sin.* 2017;30(10):1008-16.
16. Liu H, Liu Z. Evaluation of microstructures and properties of laser-annealed electroless Ni-P/Ni-Mo-P duplex coatings. *Surf Coat Tech.* 2017;330:270-6.
17. Wu Y, Wan CC, Wang YY. Fabrication of potential Ni-Mo-P diffusion barrier/seed layers for Cu inter-connects via electroless deposition. *J Electron Mater.* 2005;34(5):541-50.
18. Wang ML, Yang ZG, Zhang C, Liu DL. Growing process and reaction mechanism of electroless Ni-Mo-P film on SiO<sub>2</sub> substrate. *Trans Nonferrous Met Soc China.* 2013;23(12):3629-33.
19. Li J, Sun C, Roostaei M, Mahmoudi M, Fattahpour V, Zeng H, et al. Characterization and corrosion behavior of electroless Ni-Mo-P/Ni-P composite coating in CO<sub>2</sub>/H<sub>2</sub>S/Cl<sup>-</sup> brine: effects of Mo addition and heat treatment. *Surf Coat Tech.* 2020;403:126416.
20. Jia YP, Sun WC, Dong YR, Xiao Y, Liu JP, Zhang CX. Preparation, microstructures, and corrosion resistance of Ni-Mo-P ternary amorphous coating. *J Mater Eng Perform.* 2023;32(5):2476-8.
21. Jia YP, Sun WC, Xiao Y, Liu YW, Tian SS. Effect of rare earth on the corrosion resistance of electroless Ni-Mo-P composite coatings. *Mater Res.* 2022;25:e20210278.
22. Ishizaki T, Masuda Y, Sakamoto M. Corrosion resistance and durability of superhydrophobic surface formed on magnesium alloy coated with nanostructured cerium oxide film and fluoroalkylsilane molecules in corrosive NaCl aqueous solution. *Langmuir.* 2011;27(8):4780-8.